KeAi
CHINESE ROOTS
GLOBAL IMPACT

Available online at www.keaipublishing.com/en/journals/journal-of-magnesium-and-alloys/

ScienceDirect

Journal of Magnesium and Alloys 23 (2026) 102193

www.elsevier.com/locate/jma



Full Length Article

Suspension-calcined dolomite with ultrahigh reactivity for silicothermic magnesium production

Yingzi Ma[a], Tianyu Wang[a], Jiaqing Ye[b], Pengfei Wang[a], Chuanwei Fan[a], Yuecun Wang[a,*], Zhiwei Shan[a,*]

[a] *Engineering Research Center for Magnesium-Based New Materials, Center for Advancing Materials Performance From the Nanoscale (CAMP-Nano), State Key Laboratory for Mechanical Behavior of Materials, Xi'an Jiaotong University, Xi'an 710049, China*

[b] *Key Laboratory of Thermo-Fluid Science and Engineering, MOE, Xi'an Jiaotong University, Xi'an, Shaanxi 710049, China*

Received 3 February 2026; received in revised form 15 May 2026; accepted 16 June 2026
Available online 3 July 2026

Abstract

Calcined dolomite (CaO·MgO) is a critical feedstock for silicothermic magnesium production, and its reactivity significantly influences the primary magnesium yield. However, conventional industrial stacked-state calcination of lump dolomite often requires long residence times and results in non-uniform reactivity due to surface over-calcination and core under-calcination. While suspension calcination of powdered dolomite offers a potential route for obtaining high-reactivity feedstock at lower temperatures and shorter times, its ultimate reactivity and effectiveness in silicothermic reduction remain insufficiently explored. Here, we develop a suspension calcination route for dolomite powders and evaluate its feasibility for magnesium metallurgy through coupled simulations, laboratory experiments, and ton-scale pilot validation. Under optimized gas-solid conditions, dolomite decomposes within 8∼12 s at ∼1100 °C, producing calcined dolomite with a near-theoretical reactivity of 36.07%. This significantly outperforms typical industrial rotary kilns requiring hours of processing. This exceptional reactivity originates from a refined CaO·MgO microstructure featuring abundant mesoporosity and nanocrystalline grains. Crucially, this high-reactivity feedstock drastically improves reduction efficiency by lowering the pellet-to-magnesium mass ratio. These results demonstrate a scalable and energy-efficient pathway to produce highly reactive calcined dolomite for magnesium manufacturing.

© 2026 Chongqing University. Publishing services provided by Elsevier B.V. on behalf of KeAi Communications Co. Ltd.
This is an open access article under the CC BY-NC-ND license (http://creativecommons.org/licenses/by-nc-nd/4.0/)

Keywords: Calcined dolomite; Suspension calcination; Silicothermic magnesium production.

1. Introduction

The silicothermic process, the most extensively employed method for magnesium production, involves four key stages: dolomite calcination, raw material mixing and briquetting, vacuum reduction, and refining and casting [1–3]. Calcined dolomite (CaO·MgO) reacts with ferrosilicon (#75 SiFe) as the reductant and fluorspar (CaF_2) as the catalyst under vacuum at 1200∼1250 °C [4,5]. Although simple and well-established [6], the process is energy intensive and generates significant CO_2 emissions [7–9].

As the first step in the silicothermic magnesium production, the quality of calcined dolomite directly impacts the quality and yield of primary magnesium. Fig. 1a demonstrates the relationship between calcined dolomite reactivity and the pellet-to-magnesium mass ratio (the ratio of raw material to produced magnesium, which reflects the magnesium yield) in both laboratory and factory settings. The data show that as calcined dolomite reactivity increases, the pellet-to-magnesium mass ratio decreases. Dark green dots in the figure represent laboratory data, where reactivity increases from 25 to 33%, resulting in a reduction of the pellet-to-magnesium mass ratio from 7.4 to 5.6. In the plant, due to operational efficiency constraints, calcination reactivity ranges between 24

Peer review under the responsibility of Chongqing University.
* Corresponding authors.
E-mail addresses: yuecunwang@xjtu.edu.cn (Y. Wang), zwshan@xjtu.edu.cn (Z. Shan).

https://doi.org/10.1016/j.jma.2026.102193
2213-9567/© 2026 Chongqing University. Publishing services provided by Elsevier B.V. on behalf of KeAi Communications Co. Ltd. This is an open access article under the CC BY-NC-ND license (http://creativecommons.org/licenses/by-nc-nd/4.0/)

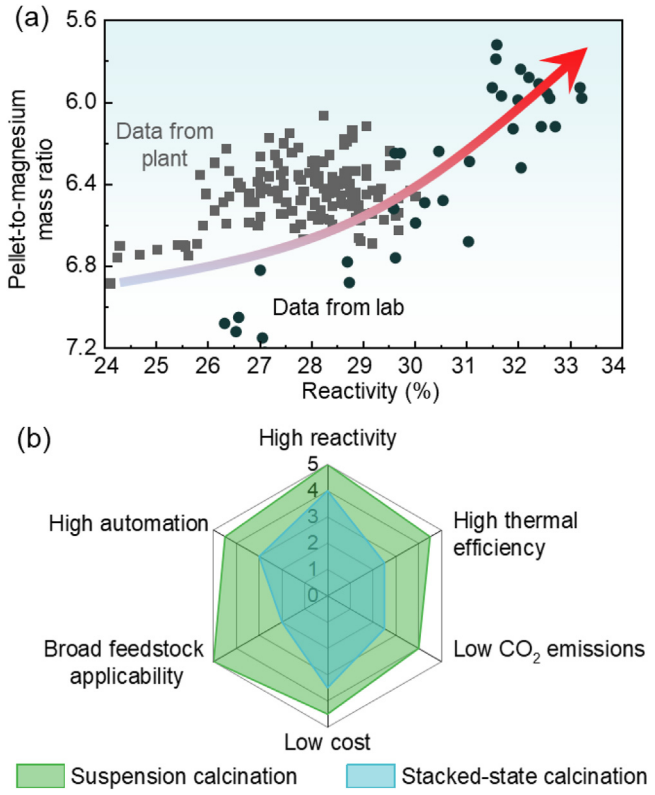


Fig. 1. (a) Relationship between calcined dolomite reactivity and the pellet-to-magnesium mass ratio (the data from plant provided by a leading primary magnesium manufacturer in China). The y-axis is inverted to highlight that a lower pellet-to-magnesium mass ratio corresponds to higher magnesium yield and better reduction efficiency; (b) Comparison of stacked-state calcination and suspension calcination.

and 31%, with a similar inverse relationship between reactivity and the pellet-to-magnesium mass ratio. Notably, the calcination stage accounts for over 30% of the total energy consumption in magnesium production and is one of the primary sources of CO_2 emissions [10,11]. Thus, optimizing the calcination process to generate high-quality feedstock at the outset is crucial for advancing the sustainable and environmentally responsible advancement of the magnesium industry [1].

In conventional rotary kiln calcination, dolomite particles (2∼4 cm) are charged in bulk into the kiln, where particle cascading and enhances heat transfer from high-temperature flue gas, producing calcined dolomite that is subsequently ground and briquetted for reduction [12,13]. However, the bulk and lump based heat transfer mode leads to low thermal efficiency and high specific energy consumption, typically necessitating temperatures above 1300 °C and extended residence times of several hours [14,15]. Radial heat transfer limitations result in asynchronous heating and decomposition, with rapid decomposition at the particle surface but insufficient heating at the core. Fractions of 8∼17% often exhibit both over- and under-calcination, with over-calcination at the exterior and under-calcination at the core. Based on its calcination characteristics, this method can be referred to as stacked-state calcination (SSC). Substandard calcined dolomite fails to fully participate in the silicothermic reduction, directly diminishing magnesium yield and product quality, while indirectly increasing residual MgO in the slag [16–18]. Elevated MgO content hinders slag reutilization because moisture absorption leads to volume expansion and cracking in construction applications. Additionally, rotary kiln calcination demands precise control over the particle size and mechanical strength of the dolomite feedstock. Production data indicate that >40% of raw materials fail to meet the necessary specifications [19]. The mining of high-quality dolomite has been heavily restricted amidst increasingly stringent environmental protection policies. As a result, the dolomite ore market suffers from shortages and inconsistent quality, not only drives a continuous increase in raw material procurement costs, but also significantly undermines the stability of the raw material supply chain. The suspension of dolomite production in Wutai, Shanxi Province, a key source of raw material, has directly triggered fluctuations in magnesium prices [20].

Given the slow heat transfer characteristics of bulk materials during stacked-state calcination, we propose reducing the particle size and adopting a more dispersed calcination approach. Suspension Calcination (SuC) is a rapid and efficient calcination technology applied in industries like cement and magnesite processing [21–24], featuring high heat transfer efficiency, stable product quality, and a compact system design [24–26]. Micron-sized particles are suspended in a high-temperature gas stream, enhancing gas-solid contact, eliminating temperature gradients, and enabling rapid decomposition while minimizing agglomeration and mass-transfer limitations [22,27,28]. The calcined products are cooled and separated from the exhaust gas by cyclones, enabling complete decomposition and proper dolomite formation in short residence times. In contrast, rotary kiln calcination is limited by heat-transfer inefficiencies, preventing full decomposition of dolomite lumps [29]. SuC integrates effortlessly into existing process routes. Fines, tailings, and mechanically weak ores, which are unsuitable for rotary kilns, can be utilized, thereby achieving nearly complete raw material utilization [30,31]. Based on these principles, our previous studies have systematically demonstrated the technical, environmental, and economic advantages of SuC, including a theoretical energy savings exceeding 50%, CO_2 emission reductions of >20%, and a production cost decrease of approximately 35% compared with rotary kilns [32,33]. Due to the highly integrated and sealed design of the suspension calcination system, only a small number of personnel are required to operate the system, greatly reducing personnel dependency. In view of the above characteristics, we conducted a comprehensive comparison between stacked-state calcination and suspension calcination, as shown in Fig. 1b. However, unlike conventional applications that focus primarily on decomposition, calcined dolomite for silicothermic magnesium production requires strict control of reactivity. Consequently, existing experience cannot be directly applied, and the reactivity and reducibility of the calcined dolomite produced by suspension calcination still require systematic experimental verification.

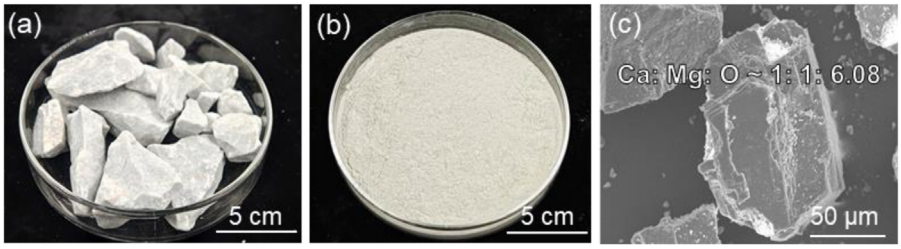


Fig. 2. The morphology of raw dolomite. (a) Dolomite lumps; (b) Crushed dolomite powders; (c) Representative SEM image of the individual dolomite microparticles.

High-reactivity calcined dolomite was prepared via suspension calcination in this work. A self-developed laboratory-scale suspension calcination apparatus was combined with numerical simulations to optimize key process parameters, enabling the preparation of calcined dolomite with a maximum reactivity of ~36%. The reactivity, microstructure, and phase composition of calcined dolomite obtained by suspension calcination were systematically compared with those from stacked-state calcination. After briquetting, the calcined dolomite was subjected to silicothermic reduction to assess the effect of calcination method on reduction performance. In addition, ton-scale calcination and kilogram-scale reduction experiments were conducted to verify scalability. This study provides a solid foundation for the application and industrialization of suspension calcination in the production of highly reactive calcined dolomite for the silicothermic magnesium process.

2. Results and discussion

2.1. Dolomite characterizations

The raw materials used in the experiments included dolomite sourced from Wutai, Shanxi Province, 75# ferrosilicon, and fluorite powder, which were supplied by Fugu Taida Coal Chemical Co., Ltd. Fig. 2a shows the macroscopic morphology of the lump dolomite, which appears grayish white with a typical carbonate mineral texture and particles on the centimeter scale. The dolomite powders obtained after crushing and grinding the raw dolomite present fine grayish white powdery appearance, serving as the feedstock for the subsequent suspension calcination. Fig. 2c displays a Scanning Electron Microscope (SEM) image of the dolomite powder, revealing a stacked platelet-like morphology. Energy-dispersive Spectroscopy (EDS) analysis indicates a Ca/Mg atomic ratio of approximately 1:1, consistent with the compositional requirements of dolomite used in the silicothermic magnesium reduction.

The chemical composition of the dolomite is listed in Table 1. The dolomite composition meets the requirements for magnesium production via the silicothermic route, with SiO_2 constituting the principal impurities.

Calcined dolomite powders were prepared by two different routes: stacked-state calcination (SSC) and suspension calcination (SuC). For SSC, although the muffle furnace lacks the dynamic rotation and axial transport of an industrial rotary kiln, it can reproduce the radial heat-transfer constraints associated with the thickness of the material layer, making it a useful laboratory-scale approach for revealing the fundamental difference between bulk calcination and suspension calcination rather than fully replicating the dynamic rotary-kiln process. Dolomite lumps were calcined in a muffle furnace at 1100 °C for 2 h, followed by crushing and sieving through a 150 μm mesh. For SuC, dolomite lumps were first crushed and sieved to obtain powders with particle sizes below 150 μm, which were then calcined for several seconds in a self-developed suspension calcination apparatus to produce calcined dolomite powders. The reactivity of calcined dolomite, k_a, was evaluated using a standard hydration-based reactivity test, which reflects the ability of MgO and CaO to react with water [34]. A total of 3.0 ± 0.001 g of calcined dolomite powder was mixed with 5 mL of deionized water and allowed to react completely, followed by drying at 150 °C for 1.5 h in an oven, as shown in Eq. (1):

$$k_a = \frac{m_2 - m_1}{m_1} \times 100\% \quad (1)$$

where m_1 is the mass of the weighed calcined dolomite powder (g), and m_2 is the mass of the product after reaction and drying (g).

Table 1
The chemical composition of dolomite based on X-ray Fluorescence Spectrometer (XRF).

Component	CaO	MgO	SiO_2	Fe_2O_3	Al_2O_3	MnO
Mass fraction (%)	30.6900	20.8400	0.6100	0.1520	0.1060	0.0077

For the silicothermic process, the molar ratio of MgO to Si was set at 2:1. Considering reaction efficiency, the mass ratio of calcined dolomite, to ferrosilicon and fluorite powder was 82.6:14.2:1.2 [35]. The raw materials were briquetted into cylindrical pellets with a diameter of 30 mm under a constant briquetting pressure of 98 MPa. The pellets were subjected to silicothermic reduction at 1250 °C under a vacuum of <10 Pa for 2 h. The pellet-to-magnesium mass ratio (*P/Mg* ratio) is defined as the mass ratio between the raw materials and the final yield of crude magnesium. It serves as a quantitative indicator of magnesium reduction efficiency and reflects the reduction reactivity of feedstocks such as calcined dolomite. Laboratory-scale reduction experiments are commonly evalu-

ated by calculating the *P/Mg* ratio based on the mass loss of the pellets. Mass-loss-based calculations may include contributions from moisture, volatile impurities, and incomplete carbonate decomposition, and therefore may overestimate magnesium yield. In this study, the pellet-to-magnesium mass ratio was calculated based on the actual mass of collected magnesium, which provides a more reliable assessment of reduction performance. Accordingly, in this study, the *P/Mg* ratio was calculated based on the mass of magnesium actually produced during the reduction reaction, providing a more reliable evaluation of reduction performance.

$$P/Mg = \frac{m_{\text{Pellet}}}{m_{\text{Mg}}} \tag{2}$$

Here, m_{Pellet} represents the mass of the pellet before reaction, and m_{Mg} denotes the mass of magnesium collected after reduction.

The morphology and phase composition of dolomite and the following calcined dolomite were characterized by Scanning Electron Microscopy (SEM, SU8230, Hitachi), X-ray Fluorescence Spectroscopy (XRF, Thermo Fisher-Arl Perform'X), X-ray Diffraction (XRD, D8 Advance A25, Bruker). The pore size distribution of calcined dolomite was determined by Brunauer-Emmett-Teller (BET, MicrotracBEL-Belsorp Max II).

2.2. Apparatus construction and parameter simulation analysis

Fig. 3a schematically illustrates the principle of suspension calcination. Powdered feedstock is entrained by the gas flow and transported into a high-temperature decomposition zone, where calcination is completed before the reacted material exits the system. Owing to the limited number of studies on suspension calcination of dolomite, particularly the lack of laboratory-scale experimental apparatus and data suitable for theoretical analysis and parameter evaluation, we independently designed a laboratory-scale suspension calcination setup comprising feeding, gas inlet, decomposition, and separation units. Based on preliminary experimental results, the calcination temperature was initially set at 1000 °C. On this basis, subsequent investigations focused on two key operating parameters, namely the gas velocity and particle size during calcination.

Based on this process, the calcination-decomposition zone, where the dominant reactions occur, was selected as the computational domain. The decomposition section was idealized as a nonuniform cylindrical geometry with a total height of approximately 1.2 m, consisting of a main cylindrical section with a diameter of 80 mm and upper and lower transition sections simplified as converging regions with a diameter of 50 mm (Fig. 3b). A computational particle fluid dynamics (CPFD) approach was employed, in which the gas phase was modelled using a Eulerian framework, while solid particles were treated in a Lagrangian method to simulate gas-solid flow and the thermochemical transformation of dolomite particles [36]. Dolomite decomposition was modeled using an apparent heterogeneous kinetic model based on the particle decomposition degree, assuming uniform particle temperature and neglecting internal gas phase diffusion resistance. Radiative heat transfer between the reactor walls and the gas particle phases was included, whereas inter-particle radiation was neglected. A uniform-velocity inlet boundary condition was applied at the bottom of the computational domain, with the inlet gas temperature set to ambient conditions, while a pressure outlet boundary condition was imposed at the top, allowing particles to exit the domain. Because dolomite undergoes a mass change upon decomposition, the extent of decomposition was determined by quantifying the mass loss of dolomite collected after 30 s of calcination as it exited the system.

Fig. 3c shows the calculated decomposition degree of dolomite particles of varying sizes at gas velocities of 0.3, 0.6, and 0.8 m/s. Overall, both gas velocity and particle size exert a pronounced influence on decomposition behavior. At a low gas velocity of 0.3 m/s, the decomposition degree initially increases and then decreases with increasing particle size. Fine particles (20∼30 μm) are readily entrained into the high-temperature zone and can maintain a quasi-stable suspension, enabling effective decomposition. In contrast, when the particle size exceeds 30 μm, the gas velocity becomes insufficient to sustain suspension, resulting in particle settling in the lower region of the reactor, shortened residence time, and limited heat exposure, which markedly reduces the decomposition degree. At a high gas velocity of 0.8 m/s, the decomposition degree increases monotonically with particle size. Fine particles are rapidly swept out of the reaction zone, leading to extremely short residence times and incomplete decomposition. In contrast, larger particles, owing to their higher inertia, remain in the high-temperature region for longer durations and sustain a more stable suspension, thereby enhancing decomposition.

At an intermediate gas velocity of 0.6 m/s, a favorable balance is achieved among particle entrainment, residence time, and heat-transfer efficiency. Small particles are rapidly entrained and leave the calciner within approximately 2 s. Although they heat up quickly, their residence time in the high-temperature zone is too short for complete decomposition. In contrast, large particles are difficult to fully suspend and remain mainly in the lower region of the calciner, where the temperature and heat-transfer efficiency are relatively low. Medium-sized particles, especially those in the range of 30∼80 μm, can maintain a more stable suspension within the high-temperature decomposition zone, enabling sufficient residence time and efficient heat transfer. Therefore, 0.6 m/s was identified as the optimal gas velocity, and a particle size of ∼75 μm was selected for subsequent simulations.

Fig. 3d presents snapshots of the instantaneous temperature fields and the temporal evolution of particle suspension under the optimized operating conditions. At the initial stage (t = ∼1 s), the introduction of ambient temperature gas creates a distinct low-temperature zone near the reactor inlet, where particle dispersion remains limited. Under these conditions, the surrounding gas temperature and velocity are low, convective heat transfer is weak, and particle tempera-

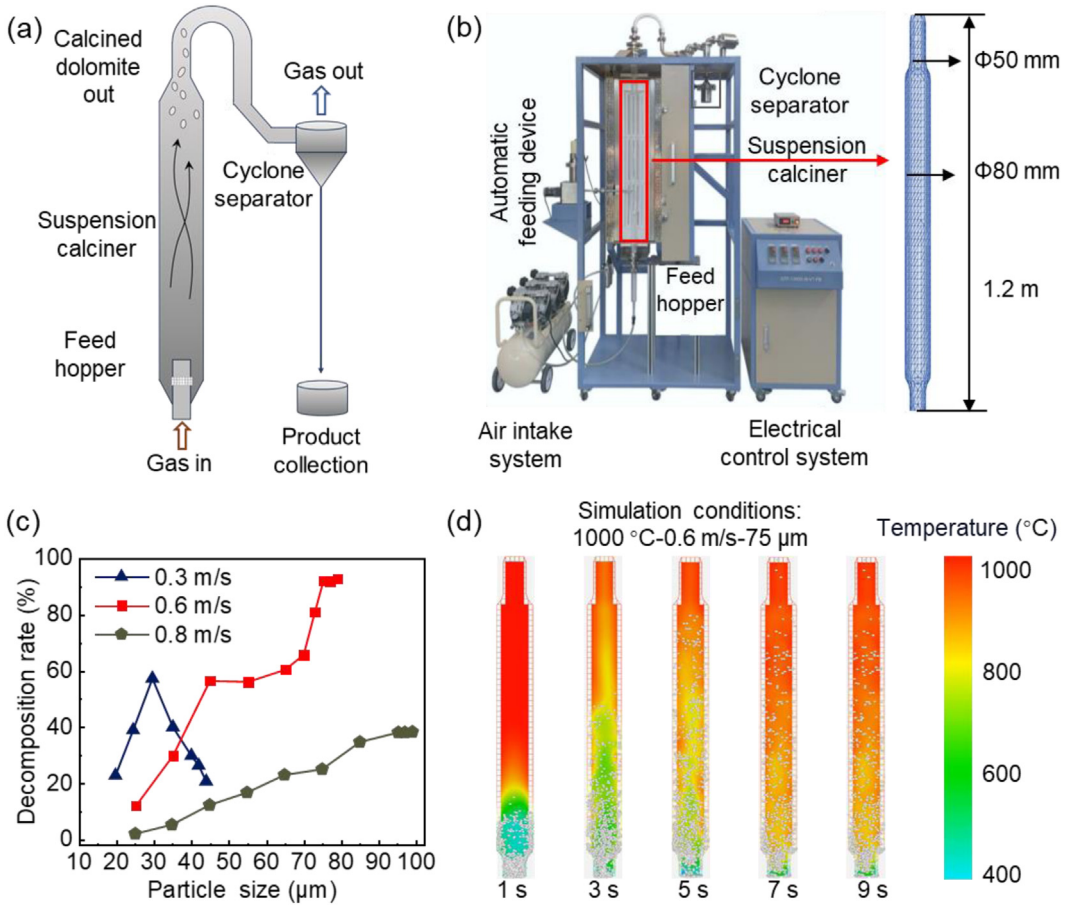


Fig. 3. Numerical simulation of the suspension calcination process in the self-developed apparatus. (a) Schematic illustration; (b) Computational model; (c) Decomposition rate under different gas velocities; (d) Suspension calcination behavior under optimized conditions.

tures and reaction rates remain limited. As time progresses to $t = 3\sim5$ s, a pronounced axial temperature gradient develops, with lower temperatures at the bottom and higher temperatures at the top of the reactor. Particles gradually disperse within the reactor, accompanied by increased gas temperature and velocity. At $t = 7\sim9$ s, particles form a relatively stable suspension state, with the particle distribution extending over nearly the entire reaction zone, where particle temperatures are high and decomposition proceeds rapidly. Finally, as the reaction progresses and particle mass continuously decreases, the fully decomposed particles exit the reactor and are collected.

Overall, the matching between gas velocity and particle size not only enhances the uniformity of particle suspension but also governs the residence time of particles in the high-temperature zone, thereby affecting heat-transfer efficiency and the final decomposition degree.

2.3. Effect of calcination process on the reactivity of calcined dolomite

Based on the calcination conditions suggested by numerical simulations, process parameters were further optimized by considering heat-transfer characteristics of the experimental apparatus. Considering heat-transfer losses in the laboratory apparatus, the furnace temperature was set to 1100 °C, at which the measured reaction-zone temperature reached ~1000 °C after 1h of holding. The gas velocity was adjusted to ~0.65m/s to accommodate practical fluctuations during feeding and gas-solid interaction. As a result, the optimized conditions employed particles with an average diameter of ~70 μm (Table 2) and a suspension velocity of ~0.65m/s at 1100 °C.

Table 2
Dolomite particle size distribution.

Particle size range (μm)	<30	30~40	40~50	50~60	60~70	70~80	80~90	>90
Mass fraction (%)	3.5	8.2	12.5	18.1	22.3	19.7	13.4	2.3

As shown in Fig. 4a, the reactivity of calcined dolomite increases rapidly with suspension calcination time, reaching the qualification threshold for the silicothermic magnesium process (≥30%) within approximately 8s. At a residence time of ~12s, the reactivity attains 36.07%, approaching the theoretical maximum of 36.33%, indicating near-complete activation of the calcined dolomite. Notably, extending the calcination time to 24s, the reactivity remains above 30%, with no decline associated with over-calcination, indicating a high degree of

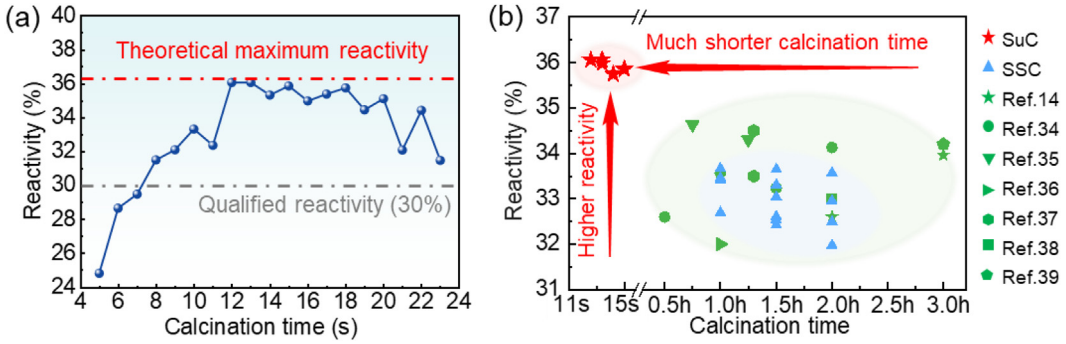


Fig. 4. Reactivity of calcined dolomite as a function of calcination time. (a) Reactivity of calcined dolomite obtained under the optimized process. The dashed red line indicates the theoretical maximum reactivity, while the dashed gray line marks the minimum qualified reactivity (~30%) required for silicothermic magnesium production; (b) Comparison of reactivity versus calcination time for SuC and SSC.

operational flexibility and tolerance of the suspension calcination system.

Fig. 4b further underscores the advantage of SuC by comparing its performance with stacked-state calcination (SSC), including representative literature data. Under comparable feed compositions, SSC consistently yields lower reactivity and fails to approach the theoretical limit, likely owing to extended heat-transfer paths and restricted CO_2 release within dolomite lumps. Even with prolonged calcination times of 1~2 h, SSC reactivity remains limited to 28~34.5% [37–42]. In contrast, suspension calcination achieves near-theoretical reactivity within seconds, reflecting fundamentally more efficient gas-solid heat transfer and rapid CO_2 release. These features promote completer and more uniform dolomite decomposition, thereby enabling exceptionally high reactivity that is difficult to realize with conventional packed or stacked calcination routes.

Overall, these results demonstrate that suspension calcination can rapidly deliver near-theoretical reactivity, whereas conventional stacked-state calcination cannot attain comparable performance through adjustments in temperature or time, thereby experimentally validating the advantages of suspension calcination for feedstock preparation in the silicothermic magnesium production.

SEM images in Fig. 5 demonstrate a clear and systematic morphological evolution of dolomite with increasing decomposition degrees. At low reactivity (~10.03%), the particles retain dense, blocky morphologies with relatively smooth surfaces, indicating limited decomposition and minimal structural disruption. Only sparse nanoscale particulates are observed on the surface, suggesting that the carbonate matrix remains largely intact. As the decomposition progresses to intermediate levels (~15.11 and ~32.89%), the original dense morphology is progressively broken down. At near-theoretical reactivity (~36.06%), the calcined dolomite exhibits a uniformly nanocrystalline morphology composed of densely packed grains with characteristic sizes on the order of tens of nanometers. The original grain boundaries are no longer discernible, indicating nearly complete decomposition and reorganization into highly reactive CaO·MgO. Upon further calcination (~31.41 and ~30.12%), slight grain coarsening and local sintering become evident. Although the material remains highly active, adjacent nanoparticles begin to neck and coalesce, leading to a broader grain size distribution and partial densification.

To further elucidate the reactivity states of calcined dolomite, under-calcination, proper-calcination, and over-calcination samples were systematically characterized. As revealed by the XRD patterns in Fig. 5b, dolomite exhibits distinctly different phase transformation behaviors at various calcination degrees. The under-calcination sample contains residual dolomite together with partially formed CaO and MgO, indicating insufficient calcination temperature or residence time that prevents complete decomposition. In contrast, the diffraction peaks of the proper-calcination and over-calcination samples are dominated by oxide phases derived from dolomite decomposition. Notably, the peaks of the over-calcination sample are sharper, suggesting further grain growth and densification under high-temperature conditions. These trends are further supported by SEM analysis. The under-calcination sample retains large, blocky dolomite particles, implying limited internal diffusion and incomplete decomposition. The proper-calcination sample consists of fine, uniformly distributed particles with a typical porous and loose morphology, whereas the over-calcination sample exhibits pronounced grain coarsening and sintering, accompanied by a significant reduction in porosity and densified interparticle interfaces.

The BET test measures the surface area and pore characteristics of materials by adsorbing gas at liquid nitrogen temperature and analyzing adsorption at different pressures. Fig. 6 summarizes the BET characterization results of calcined dolomite with different calcination states, providing quantitative insight into surface area, pore structure, and microstructural evolution. All samples were prepared at 1100 °C using the self-developed suspension calcination apparatus, with different residence times. The under-calcination samples had reactivities of 10.03 and 15.11%, the proper-calcination samples had reactivities of 36.06 and 36.00%, and the over-calcination samples had reactivities of 28.93% and 31.41%, respectively. Fig. 6a shows the N_2 adsorption-desorption isotherms. All samples exhibit typical mesoporous characteristics, with evident hysteresis loops arising from capillary condensation.

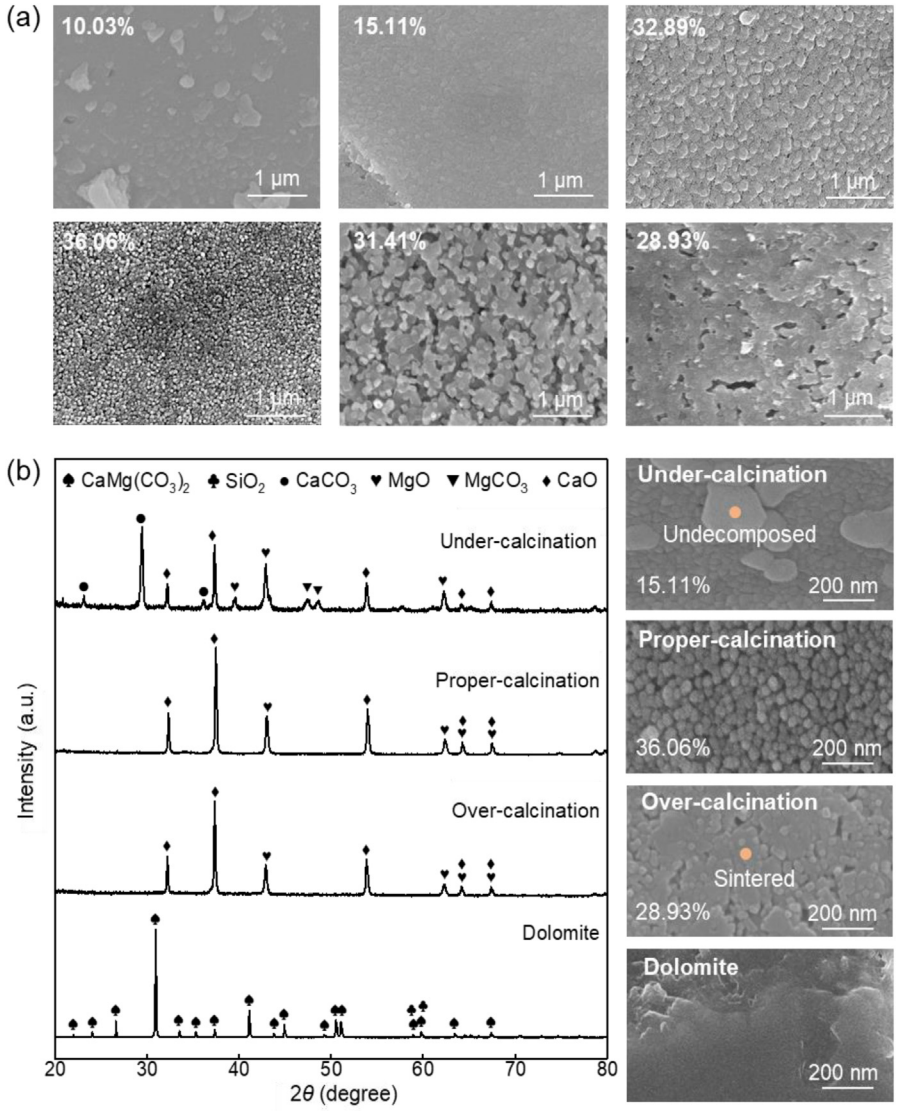


Fig. 5. (a) SEM images showing the surface morphology suspension-calcined dolomite with different reactivity levels, corresponding to under-calcination, proper-calcination, and over-calcination. (b) XRD patterns of under-, properly- and over- suspension-calcined dolomite, together with the un-calcined dolomite powder. Right panel: Enlarged SEM images corresponding to each calcination state.

However, the adsorption capacity and hysteresis behavior vary markedly with calcination degree. The under-calcination sample displays relatively limited adsorption, indicating incomplete pore development, whereas the proper-calcination sample shows the highest adsorption volume over the entire relative pressure range, reflecting a well-developed porous network. In contrast, the over-calcination sample exhibits reduced adsorption at high relative pressures, suggesting partial pore collapse or sintering induced densification. Fig. 6b compares the corresponding specific surface areas. The surface area increases sharply from the under-calcination state to the under-calcination state, reaching a maximum under optimal calcination conditions. This enhancement arises from effective decarbonation and decomposition into fine CaO·MgO. Upon over-calcination, the specific surface area decreases noticeably, consistent with grain growth and pore coalescence that reduce the accessible surface.

Fig. 6c∼e further elucidate the evolution of grain size distribution and pore size. The grain size distribution reflects nucleation and growth behavior as well as microstructural evolution, while the pore size distribution, expressed as dV/dlog(D), represents the incremental pore volume contribution within each logarithmic pore size interval. In the under-calcination sample (Fig. 6c), the pore size distribution is relatively narrow and skewed toward smaller pores, accompanied by comparatively large crystallite sizes, indicating limited decomposition and insufficient pore generation. For the proper-calcination sample (Fig. 6d), the distribution shifts to a well-defined mesoporous regime and the average pore diameter increases to an optimal, moderate value, indicating efficient CO_2 release and the formation of interconnected transport pathways. The proper-calcination sample exhibits a narrow and symmetric grain size distribution centered at 40∼60 nm, indicating uniform grain size. Its pore volume is mainly contributed by

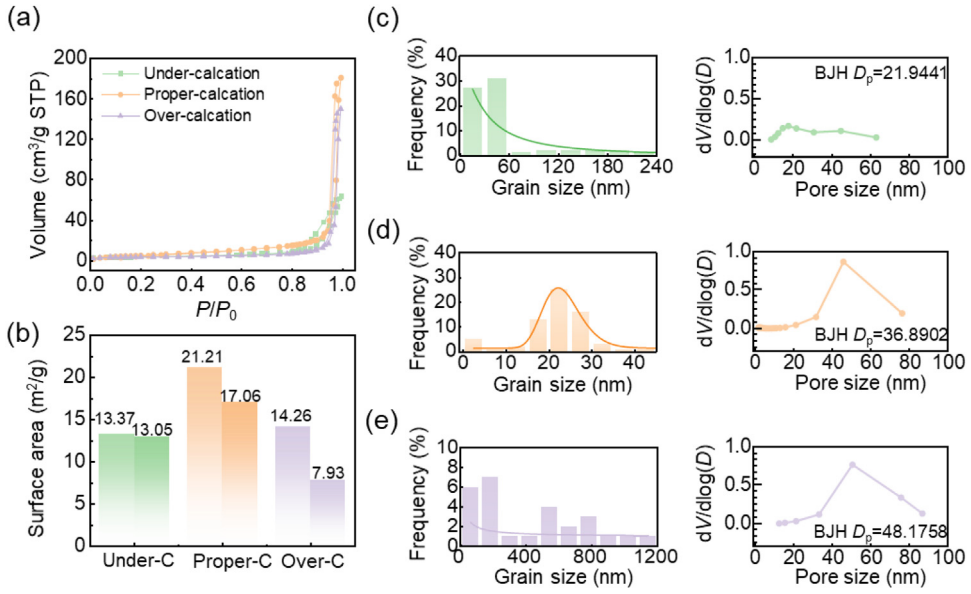


Fig. 6. BET analysis of calcined dolomite at different calcination states. (a) N_2 adsorption-desorption isotherms; (b) Corresponding BET specific surface areas; (c–e) Pore size distributions derived from adsorption data and grain size statistics for (c) under-calcined, (d) properly calcined, and (e) over-calcined dolomite samples.

pores smaller than 50 nm, suggesting a homogeneous microporous structure. This behavior can be attributed to the uniform release of CO_2 during dolomite decomposition, which promotes the formation of a well-connected porous network with moderate pore sizes and facilitates rapid gas diffusion and mass transfer, consistent with the SEM observations. In the over-calcination sample (Fig. 6e), the pore size distribution shifts toward larger pores, reflecting pore coarsening and particle coalescence driven by prolonged high-temperature exposure. Most grains exceed 200 nm, and the pore size distribution becomes flatter, reflecting pore coalescence caused by grain growth and sintering at elevated temperatures. Consequently, the number of fine pores decreases, while larger pores become more prevalent, leading to reduced pore uniformity.

Overall, proper-calcination dolomite exhibits fine and uniformly distributed grains and pores, providing abundant reactive sites and facilitating rapid diffusion of reactant gases. Therefore, achieving a proper-calcination state through precise control of temperature and residence time in suspension calcination is essential for producing highly reactive calcined dolomite.

2.4. Effect of calcination process on the reduction performance of calcined dolomite

To evaluate the practical performance of suspension calcined dolomite in the silicothermic magnesium production, reduction experiments were conducted using a self-developed laboratory-scale silicothermic reduction apparatus.

Fig. 7a shows the purity of crude magnesium produced using calcined dolomite prepared by SuC and SSC. The magnesium obtained from suspension calcined feed exhibits a slightly higher purity. This difference is most plausibly attributed to the mechanical fragmentation and subsequent sieving during suspension processing, which can partially remove impurity-rich fractions. Importantly, the comparison demonstrates that suspension calcination does not introduce additional impurities into the system, confirming its chemical compatibility with downstream magnesium production.

The reduction behavior of calcined dolomite produced by SuC was systematically compared with that obtained by conventional SSC. As shown in Fig. 7b, the average *P*/*Mg* ratio for calcined dolomite prepared by SSC approximately 6.1, whereas that of SuC dolomite is reduced to 5.7, with a minimum of 5.54, indicating a significantly improved magnesium yield. This improvement suggests that suspension calcination provides a higher fraction of highly reactive MgO capable of participating effectively in the silicothermic reduction, thereby enhancing resource utilization efficiency from the feedstock stage. The residual MgO content in the reduction slag was further quantified to elucidate the underlying mechanisms. Calcined dolomite produced by SSC typically suffers from both over-calcination and under-calcination. Over-calcination leads to MgO grain coarsening, reduced specific surface area, and decreased reactivity, rendering part of the MgO ineffective during reduction. In contrast, under- calcination fractions contain undecomposed dolomite, which must decompose again during reduction, leading to additional heat consumption and prolonged reaction time. Moreover, CO_2 released during secondary decomposition consumes ferrosilicon reductant, reducing the effective reductant availability and ultimately lowering magnesium yield. In comparison, under SuC conditions, the residual MgO content in the slag after reduction is below 3%, representing a 47.3% reduction relative to the SSC process. This value satisfies the national standard for reduction slag used as construction materials (MgO <5%), enabling direct

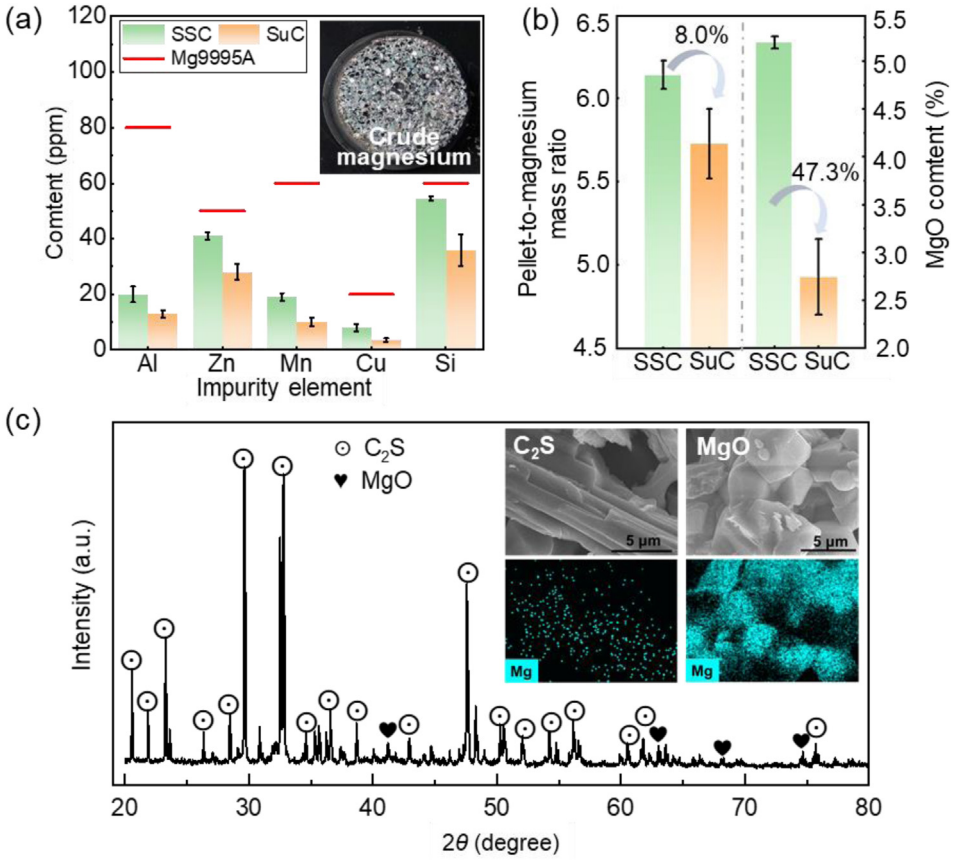


Fig. 7. Reduction performance of high-reactivity calcined dolomite in the silicothermic process. (a) Chemical purity of the obtained crude magnesium; (b) Comparison of pellet-to-magnesium mass ratio and residual MgO content for SSC and SuC; (c) XRD pattern and corresponding SEM images of the reduction slag, together with elemental mapping of Mg.

reutilization of the by-product and improving the overall environmental and economic performance of the process. Fig. 7c presents the characterizations of the reduction slag, whose main constituent is $2CaO{\cdot}SiO_2(C_2S)$, revealing that the dominant crystalline phases are C_2S and residual MgO. The absence of unexpected phases further confirms that the suspension calcination route does not alter the fundamental reaction pathway or introduce parasitic reactions. SEM images show plate-like C_2S crystals and angular MgO particles, while corresponding elemental mapping confirms their distinct spatial distributions. The coexistence of well-defined C_2S and MgO phases indicates a clear separation between reaction products and unreacted residues.

Following the laboratory-scale validation of feasibility and performance advantages, ton-scale industrial pilot calcination experiments were further carried out, accompanied by reduction tests in an industrial reduction furnace. The industrial suspension-calcination system consists of a three-stage preheating unit, a decomposition furnace, cyclone separation, gas recirculation, dust collection, and product collection units. Dolomite powder was preheated to above 800 °C and then calcined in the decomposition zone within ~10 s at 1000 ± 30 °C. Considering the relatively high ambient humidity, the product reactivity was controlled at ~31%, which still meets the requirement for silicothermic magnesium production. Calcined dolomite produced on-site, the industrial reduction furnace after reduction, and the kilogram-scale crude magnesium obtained. The crude magnesium produced in the industrial trials exhibits a pellet-to-magnesium mass ratio of 6.1, which is superior to the current industry average (6.2–6.7) [43–45]. These results demonstrate the stable scalability and strong engineering application potential of suspension calcination for the preparation of silicothermic magnesium feedstock from laboratory to industrial scale.

Overall, the present results demonstrate that suspension calcination of dolomite is a feasible and highly advantageous route for producing high-quality calcined dolomite for the silicothermic magnesium process. In response to practical concerns widely recognized in industry, such as the hygroscopic nature and storage instability of calcined dolomite powders, preliminary exploratory studies have been conducted to analyze moisture absorption behavior and its evolution, and corresponding mitigation strategies have been tentatively proposed. Future work will focus on the moisture absorption mechanisms of calcined dolomite, the influence of environmental factors, and their effects on reactivity and reduction performance, with the aim of developing robust anti-hygroscopic and storage-stabilization strategies to support the engineering application of suspension calcination under diverse regional and operational conditions.

3. Conclusions

Suspension calcination enables the production of calcined dolomite with ultrahigh reactivity of 36.07%, approaching the theoretical limit and significantly exceeding that achieved by conventional stacked-state calcination. When applied to the silicothermic magnesium reduction, this highly reactive feedstock markedly improves reduction efficiency, lowering the pellet-to-magnesium mass ratio to as low as 5.54. Ton-scale pilot calcination and subsequent industrial reduction trials further demonstrate the stability and scalability of the proposed approach. The markedly enhanced reactivity of suspension-calcined dolomite is attributed to its refined microstructure, characterized by nano grains, pronounced mesoporosity, and a large specific surface area, which together provide abundant reactive sites, facilitate efficient gas-solid reactions, and promote rapid magnesium vapor release during reduction. Suspension calcination thus offers an energy-efficient route and a viable technical foundation for improving the sustainability and competitiveness of silicothermic magnesium production.

Data availability

Data will be made available on request.

Declaration of competing interest

Zhiwei Shan is an editorial board member for Journal of Magnesium and Alloys and was not involved in the editorial review or the decision to publish this article. All authors declare that there are no competing interests.

CRediT authorship contribution statement

Yingzi Ma: Writing – original draft, Visualization, Methodology, Investigation, Formal analysis, Data curation. **Tianyu Wang:** Visualization, Methodology, Formal analysis. **Jiaqing Ye:** Software. **Pengfei Wang:** Resources. **Chuanwei Fan:** Investigation. **Yuecun Wang:** Writing – review & editing, Supervision, Conceptualization. **Zhiwei Shan:** Writing – review & editing, Conceptualization.

Acknowledgments

Zhiwei Shan and his team members appreciate the supporting by the National Natural Science Foundation of China (Grant No. U24A2021) and Xianyang High-tech Industrial Development Zone, also FuGu TaiDa Coal Chemical Co., Ltd. for providing the experiment materials.

References

[1] D. Wang, T. Zhang, J. Xu, K. Wang, J. Magnes. Alloys 13 (2025) 2470–2499, doi:10.1016/j.jma.2025.04.013.
[2] J. Zhang, J. Miao, N. Balasubramani, D.H. Cho, T. Avey, C.-Y. Chang, A.A. Luo, J. Magnes. Alloys 11 (2023) 3867–3895, doi:10.1016/j.jma.2023.11.007.
[3] Y. Yuan, et al., J. Magnes. Alloys 13 (2025) 4689–4732, doi:10.1016/j.jma.2025.09.034.
[4] M uğdayci, A Turan, M Alkan, et al., in: Magnesium production from calcined dolomite via the pidgeon process[M].Magnesium and Its Alloys, CRC Press, 2019, pp. 47–56.
[5] D. Hou, et al., Appl. Therm. Eng. 236 (2024) 121885, doi:10.1016/j.applthermaleng.2023.121885.
[6] X. Feng, et al., J. Magnes. Alloys 17 (2026) S2213956725001720, doi:10.1016/j.jma.2025.05.001.
[7] J. Xu, T. Zhang, X. Li, Materials (Basel) 16 (2023) 3340, doi:10.3390/ma16093340.
[8] X. Li, T. Zhang, Y. Liu, J. Guo, J. Xu, Y. Liang, J. Magnes. Alloys 13 (2025) 3134–3149, doi:10.1016/j.jma.2024.06.027.
[9] S. Zhang, et al., J. Magnes. Alloys 11 (2023) 3710–3723, doi:10.1016/j.jma.2022.02.003.
[10] J. Xu, T. Zhang, Y. Liu, Y. Liu, J. Env. Manage. 373 (2025) 124000, doi:10.1016/j.jenvman.2024.124000.
[11] F. Gao, et al., Trans. Nonferrous Met. Soc. China 18 (2008) 749–754, doi:10.1016/S1003-6326(08)60129-6.
[12] Y. Wada, S. Fujii, E. Suzuki, M.M. Maitani, S. Tsubaki, S. Chonan, M. Fukui, N. I-nazu, Sci. Rep. 7 (2017) 46512, doi:10.1038/srep46512.
[13] Y. Deng, et al., J. Clean Prod. 363 (2022) 132640, doi:10.1016/j.jclepro.2022.132640.
[14] R. Xu, H. Yuan, Light Met. (1990) 40–44, doi:10.13662/j.cnki.qjs.1990.07.012.
[15] G. Jia, Light Met. (1998), doi:10.13662/j.cnki.qjs.1998.10.010.
[16] Y. Zhai, L. Huang, C. Wu, L. Jin, Constr. Build. Mater. 504 (2025) 144647, doi:10.1016/j.conbuildmat.2025.144647.
[17] E. Bernard, et al., Cem. Concr. Res. 186 (2024) 107655, doi:10.1016/j.cemconres.2024.107655.
[18] X. Wu, Bricks Tiles (2025) 24–28, doi:10.16001/j.cnki.1001-6945.2025.08.006.
[19] J. Bojanovský, V. Máša, I. Hudák, P. Skryja, J. Hopjan, Rotary Kiln, a unit on the border of the process and energy industry—current state and perspectives, sustainabi-lity 14 (2022) 13903. https://doi.org/10.3390/su142113903.
[20] Fugu Magnesium & Fugu Magnesium Association, Fugu Magnes. (2025) https://mp.weixin.qq.com/s/PVkF84tJ8Ms_WOorlQK-JQ. accessed 12 January 2026.
[21] H.A.M. Ahmed, M.S. Alhaddad, Eng. Mohammed S, Alhaddad (2022).
[22] Y. Zhang, L. Zhang, H. pang, Cem. Eng. (2024) 16–19, doi:10.13697/j.cnki.32-1449/tu.2024.01.005.
[23] B. Zhao, Y. Chen, Inorg. Chem. Ind. 45 (64) (2013) 38–40, doi:10.3969/j.issn.1006-4990.2013.11.011.
[24] H. Zhang, et al., Processes 12 (2024) 550, doi:10.3390/pr12030550.
[25] Q. Li, et al., Inorg. Chem. Ind. 46 (71) (2014) 30–33, doi:10.3969/j.issn.1006-4990.2014.10.007.
[26] Y. Chen, Z. Tian, B. Zhao, Bull. Chin. Ceram. Soc. 33 (2014) 1193–1197, doi:10.16552/j.cnki.issn1001-1625.2014.05.038.
[27] A. Teklay, C. Yin, L. Rosendahl, L.L. Køhler, Appl. Clay Sci. 103 (2015) 10–19, doi:10.1016/j.clay.2014.11.003.
[28] S. Xu, et al., Cem. Guide New Epoch 29 (2023) 51–56, doi:10.16008/j.cnki.1008-0473.2023.02.011.
[29] V. Meyer, A. Pisch, K. Penttilä, P. Koukkari, Chem. Eng. Res. Des. 115 (2016) 335–347, doi:10.1016/j.cherd.2016.08.007.
[30] J. Shi, Refract. Lime 49 (2024) 50–52, doi:10.16425/j.cnki.1673-7792.2024.01.009.
[31] X. Huang, et al., J. Magnes. Alloys 17 (2026) S2213956725000817, doi:10.1016/j.jma.2025.02.025.
[32] Z. Shan, et al., Mater. China 43 (2024) 46–53, doi:10.7502/j.issn.1674-3962.202302004.
[33] Z. Shan, et al., Mater. China 43 (2024) 1053–1063, doi:10.7502/j.issn.1674-3962.202412003.
[34] R.Y Xu, Production Technology of Magnesium by Silicothermic Process, Central South University Press, Changsha, 2003.
[35] H. Liu, R. Xu, Light Met. (1997), doi:10.13662/j.cnki.qjs.1997.04.010.
[36] C. Chen, et al., Powder Technol. 235 (2013) 238–247, doi:10.1016/j.powtec.2012.10.014.

[37] Z. Shan, et al., Mater. China 43 (2024) 1053–1063, doi:10.7502/j.issn.1674-3962.202412003.
[38] Z. Qi, et al., Nonferrous Met. 61 (2009) 80–83 https://kns.cnki.net/KCMS/detail/detail.aspx?dbcode=CJFQ&dbname=CJFD2009&filename=YOUS200902021.
[39] Q. Tang, et al., Light Met. (2011) 47–51, doi:10.13662/j.cnki.qjs.2011.03.016.
[40] W. Hu, Research on Preparation of Magnesiumerr by Vacuum Thermal Reduction of Calcined Dolomite and Magnesite[D], Northeastern University, 2011.
[41] C. Zhang, C. Wang, S. Zhang, L. Guo, Int. J. Miner. Process. 142 (2015) 154–160, doi:10.1016/j.minpro.2015.01.008.
[42] Y. Bai, Y. Wang, Light Met. (1996), doi:10.13662/j.cnki.qjs.1996.08.010.
[43] Y. Wang, J. You, J. Peng, Y. Di, JOM 68 (2016) 1728–1736, doi:10.1007/s11837-016-1865-6.
[44] D.-X. Fu, et al., JOM 68 (2016) 3208–3213, doi:10.1007/s11837-016-2034-7.
[45] R. Li, F. Liu, J. Zhong, P. Yang, S. Zhang, Metall. Mater. Trans. B 52 (2021) 558–569, doi:10.1007/s11663-020-02039-9.